

Inferring radial models of mantle viscosity from gravity (GRACE) data and an evolutionary algorithm

G. Soldati^{a,*}, L. Boschi^b, F. Deschamps^b, D. Giardini^b

^a Istituto Nazionale di Geofisica e Vulcanologia, via di Vigna Murata 605, 00143 Roma, Italy

^b Institute of Geophysics, E.T.H. Hönggerberg-HPP, 8093 Zürich, Switzerland

ARTICLE INFO

Article history:

Received 6 May 2008

Received in revised form

24 November 2008

Accepted 11 March 2009

Keywords:

Mantle rheology

Inverse theory

Viscous flow

Gravity

Tomography

ABSTRACT

Convective flow in the mantle can be thought of (and modeled) as exclusively driven by density heterogeneities in the mantle itself, and the resulting lateral variations in the Earth's gravity field. With this assumption, and a model of mantle rheology, a theoretical relationship can be found between 3D mantle structure and flow-related quantities that can be measured on the Earth's surface, like free-air gravity anomalies. This relationship can be used to set up an inverse problem, with 1D mantle viscosity as a solution. In the assumption that seismic velocity anomalies be of purely thermal origin, and related to density anomalies by a simple scaling factor, we invert the large-scale length component of the above-mentioned measurements jointly with seismic observations (waveforms and/or travel times) to derive an accurate 5-layer spherically symmetric model of upper- and lower-mantle viscosity. We attempt to account for non-uniqueness in the inverse problem by exploring the solution space, formed of all possible radial profiles of Earth viscosity, by means of a non-deterministic global optimization method: the evolutionary algorithm (EA). For each sampled point of the solution space, a forward calculation is conducted to determine a map of gravity anomalies, whose similarity to GRACE (gravity recovery and climate experiment) is then measured; the procedure is iterated to convergence, according to EA criteria. The robustness of the inversion is tested by means of synthetic tests, indicating that our gravity data set is able to constrain less than 6 radial layers, each with uniform viscosity. Independently of the tomographic model or the scaling factor adopted to convert seismic velocity into density structure, the EA optimization method finds viscosity profiles characterized by low-viscosity in a depth range corresponding to the transition zone, and relatively uniform elsewhere.

© 2009 Elsevier B.V. All rights reserved.

1. Introduction

The rheology of the Earth is of central importance for understanding both the Earth's transient deformation and long-term mantle dynamics. Present-day estimates of mantle viscosity are based on experimental studies of creep mechanisms in mantle minerals and on the analysis of geophysical observations of the Earth's response to surface and internal loading: mantle convection observables (timescale $\sim 10^6$ years), post-glacial rebound data ($\sim 10^3$ years), and post-seismic relaxation (1–100 year) following major earthquakes.

Viscosity is then typically estimated after solving coupled flow and gravitational potential equations for instantaneous deformation (flow, surface deformation, geoid) or time-dependent deformation (relative sea-level, plate motions); the former

approach is sensitive to relative viscosity variations, while the latter also allows an estimate of absolute viscosity. In both cases, mantle viscosity is inferred by fitting modelled signals to various types of observations: relative sea level and variations in the Earth's rotational parameters for post-glacial rebound studies, dynamic topography, geoid and plate velocities for mantle convection analysis.

The surface observables of post-glacial rebound, geoid and dynamic topography have provided only first-order constraints on the radial viscosity structure of the mantle: while geoid/dynamic topography studies suggest that mantle viscosity increases by a factor of 30 or more from the basis of the lithosphere to the core–mantle boundary (e.g. Hager and Richards, 1989), most post-glacial rebound studies (Haskell, 1935; Peltier, 1976, 1998; Mitrovica and Peltier, 1995; Kaufmann and Lambeck, 2002) favour a moderate increase in viscosity at the upper-to-lower mantle discontinuity. These inferences are still subject of a contentious debate, and to reconcile convection-based and post-glacial rebound-based estimates, joint inversions of these two kinds of data have been performed, obtaining profiles with an overall increase in viscosity

* Corresponding author. Tel.: +39 0651860487.

E-mail address: soldati@ingv.it (G. Soldati).

towards the lower mantle (e.g. Forte and Mitrovia, 1996; Mitrovia and Forte, 2004).

Recent progress, including the introduction of compressibility (Corrieu et al., 1995; Panasyuk et al., 1996; Forte and Mitrovia, 1996), the evaluation of the performance of non-Newtonian rheology (Wu, 1992; Dal Forno et al., 2005), and the effects of laterally varying (3D) viscosity structure (Richards and Hager, 1989; Zhang and Christensen, 1993; Kaufmann and Wu, 2002; Paulson et al., 2005; Moucha et al., 2007) have not clarified the question, and the only point of general agreement is that the lower mantle is more viscous than the upper mantle.

Mantle circulation models that simultaneously predict seismic (P- and S-wave velocities) and geodynamical data (free-air gravity anomaly) have been shown to be particularly good at fitting the latter (Forte et al., 1994). Here we model viscous flow in the Earth on the basis of a wide range of possible viscosity profiles, and attempt to identify the profiles for which the modeled viscous flow does the best job of predicting observed free-air gravity anomalies from GRACE (gravity recovery and climate experiment) (Tapley et al., 2005). We define a priori density (ρ) models needed in mantle-flow calculations on the basis of seismic tomographic ones, scaled by a factor depending only on depth. This requires the assumption that the relative thermal and compositional contributions to seismic anomalies are the same everywhere at any given depth.

The interpretation of long-wavelength geoid/gravity anomalies in terms of mantle convection has a long history, starting from the pioneering works of Hager and O'Connell (1981), Ricard et al. (1984) and Richards and Hager (1984), to the recent ones by Panasyuk and Hager (2000), Forte and Mitrovia (2001) and Kaban et al. (2007). With few exceptions, authors have adopted a viscous-flow theory which assumes mantle rheology to be represented in terms of an effective viscosity varying only with depth. Although mantle viscosity is likely to have lateral variations, 1D viscosity profiles have been shown to be an adequate representation of the horizontally averaged mantle viscosity structure (Moucha et al., 2007); conversely, the effect of lateral variations in viscosity is thought to be reflected almost exclusively in the small scale (high harmonic degree) component of the gravity field. The same is true of upper-mantle viscosity, while low-degree coefficients of the gravity field are more sensitive to the lower mantle (Richards and Hager, 1989; Forte and Peltier, 1994). Our goal is to identify a 1D, whole-mantle viscosity model, and for this reason we neglect (except for a test in Section 3.3) the high-degree component of gravity data and, consequently, of seismic models.

The goal of our contribution is not only to determine the viscosity profile of the mantle, but also to estimate the ability of gravity anomalies to resolve the radial distribution of viscosity as inferred from tomography and flow models. We tested and used an evolutionary algorithm to invert various tomographic models for a radial profile of the mantle viscosity, and found that all the most likely viscosity profiles predict transition-zone (410–660 km depth) viscosity to be lower than in the uppermost and lower mantle.

2. Theory

2.1. Viscosity, gravity, and mantle flow

The relative radial variations in mantle viscosity can be determined from gravity measurements. An analytical theory of mantle flow (Ricard et al., 1984; Forte and Peltier, 1987, 1991) provides geoid kernels (G_l , with l denoting the harmonic degree) given an average density profile (here, PREM), and a prescribed viscosity profile. The surface gravity anomalies (δg_l^m , with m harmonic order) are modeled by radial integration (from top of the outer core to the surface) of the ρ anomalies ($\delta \rho_l^m$), modulated by the geoid kernels. For

each harmonic, gravity anomalies are thus given by (e.g. Forte and Peltier, 1987)

$$\delta g_l^m(\theta, \phi) = k \frac{l-1}{2l+1} \int_r G_l(v/v_0, r) \delta \rho_l^m(r, \theta, \phi) dr, \quad (1)$$

where k is a constant that depends on the Earth's radius, surface gravity acceleration, and average mantle density, v_0 is a reference value for viscosity (Forte and Peltier, 1991) and the integration is carried out over the entire depth of the mantle. The multilayer approximation is employed, in which the viscosity is assumed to be constant within each layer and discontinuous at the layer boundaries; it should be noted that only the depth variation of relative viscosity v/v_0 is needed to compute the geoid kernels.

We scale ρ anomalies from shear-velocity (v_S) ones,

$$\delta \rho_l^m(r, \theta, \phi) = \zeta(r) \delta v_{S_l}^m(r, \theta, \phi), \quad (2)$$

where the scaling factor ζ is defined by

$$\zeta(r) = \frac{\delta \ln \rho(r, \theta, \phi)}{\delta \ln v_S(r, \theta, \phi)}. \quad (3)$$

The kernels G_l are calculated following the approach of Forte and Peltier (1991), who expanded in terms of generalized spherical harmonics the constitutive equation, the conservation of mass and momentum, and solved for the poloidal flow using the method of propagator equations. The constraints arising from the observed geometry of rigid surface plates are included in a dynamically consistent manner by means of the buoyancy projection method (Forte and Peltier, 1991), in which the motions of surface plates are predicted (being coupled to the underlying mantle flow) rather than imposed. The plate geometries and corresponding projection operators are represented in terms of spherical harmonic basis functions up to degree $l = 8$, in order to reduce the effect of uncertainties in tomography (larger for higher spherical harmonic degrees), and because higher-degree geoid kernels are sensitive to heterogeneous structure in the upper mantle only, while we want to integrate ρ anomalies over the whole mantle. The mantle flow theory we employ takes into account many of the complexities of the real Earth, like sphericity, compressibility and self-gravitation, and additionally allows to compute surface dynamic topography, CMB deflections and plate motions via the surface divergence.

This approach to modeling the surface gravity field has, however, several limitations: first, as seen before, only the ratios between viscosity values at different depths can be constrained, rather than the absolute values of viscosity, thus neglecting the effects of toroidal flow and associated lateral viscosity variations. The problem is also complicated by the existence of many, competing tomographic models of seismic velocity. The amplitude and pattern of seismic velocities in the mantle are known only approximately, and despite the agreement at long wavelengths (Becker and Boschi, 2002), various tomographic images differ in shape, depth extent, and amplitude of fine features (e.g., Becker and Boschi, 2002; Romanowicz, 2003; Boschi et al., 2007). Last, establishing an appropriate velocity-to-density scaling for the mantle is not straightforward. Growing evidence suggests that seismic velocity anomalies reflect both thermal and compositional heterogeneities (van der Hilst and Karason, 1999; Karato and Karki, 2001; Deschamps et al., 2001). Unlike that of temperature variations, the effect of compositional variations on seismic velocities and density is not yet well understood. A solution to this problem is to use a density model derived from a seismic-geodynamic inversion which implicitly includes both thermal and compositional effects on buoyancy (Simmons et al., 2007).

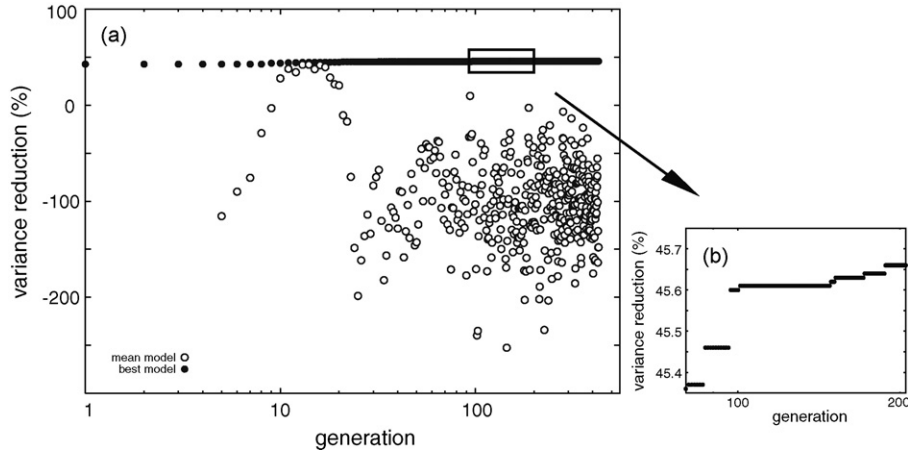


Fig. 1. Example of the performance of the EA evolving from generation 1 to 500 (a). Empty and filled circles represent the variance reduction (%) of the best-fitting model and the average fitness of the population, for each generation. The decrease in mean variance reduction at 10–20 generations corresponds to an adjustment of the mutation-rate parameter defined in Section 2.2. Fit of best model as a function of generation number (b) after 100 generations.

2.2. Evolutionary algorithms

In this study we conduct a number of inversions based on different tomographic models and different values of the ratio between density and seismic velocity, and carry out a comparative evaluation of the resulting viscosity profiles. Owing to the above factors, and to nonlinearity (geoid kernels depend on viscosity itself), the problem of finding viscosity profiles from geophysical observables does not have a unique solution. We attempt to account for non-uniqueness in the inverse problem by exploring the solution space, formed of all possible radial profiles of Earth viscosity, by means of a stochastic optimization method: the evolutionary algorithm (EA).

The first EAs, or optimization algorithms based on ideas from evolutionary theory, were conceived and implemented by Reichenberg (1973). Authors in earth sciences have already used EAs to find viscosity profiles from gravity data (King, 1995; Kido and Cadec, 1997; Kido et al., 1998), but our analysis represents an improvement in that it takes advantage of the increased power of modern calculators to explore in more detail the solution space. In particular, we have been able to quantify the resolution limit of gravity data, finding that no more than 5 independent parameters (uniform layers) describing viscosity can be reliably constrained. In addition, a systematic test of the setting parameters of our EA lead to the conclusion that while the choice of a population of 100 individuals is appropriate for this problem, the number of generations over which King (1995) based his analysis is not sufficient to grant the stability of the solution. Fig. 1 shows that after 100 generations the fit of the solution model to the data may still be improving: we thus increased the number of generations from 100 to 500.

EAs use the idea of “survival of the fittest”, to perform an iterative, multidimensional search for an optimal value of a given cost function. A typical EA requires a genetic representation of the solutions (in general, as arrays of bits), which play the role of individuals in a population. The algorithm starts from a random population whose individuals are selected according to their fitness, and the best are used to form a new population, likely to be “more fit”. Couples of parent chromosomes generate offspring by means of crossover and mutation. This procedure is repeated until a given maximum number of generations is reached, or convergence achieved. EAs are helpful because they can rapidly locate good approximate solutions to all types of problems, requiring no smoothness assumptions on the fitness function or its domain, and because of their robustness in finding global maxima in the presence of many local maxima. Furthermore, EAs are naturally parallel, thus allowing an easy optimization of machine resources.

We use Charbonneau and Knapp’s (1995), freely available PIKAIA implementation of the EA. PIKAIA incorporates two basic evolutionary operators: uniform one-point crossover, and uniform one-point mutation. The mutation rate (i.e. the chance that a random variation in an individual’s traits occurs, independent of those of the parents) can be dynamically adjusted during the evolution, using either the linear distance in parameter-space or the difference in fit between the best and median solutions in the population.

The mutation rate is a key parameter: if it is too low, the algorithm may converge prematurely to a local optimum, the EA failing to explore uniformly the space of parameters. In contrast, a high mutation rate may lead to slow or no convergence (an EA with high mutation is practically equivalent to a Monte Carlo algorithm). Charbonneau and Knapp (1995) suggest that a good compromise between allowing for new solutions and losing track of already identified ones is achieved by starting the EA run with a low mutation rate, and then allowing the mutation rate to grow as convergence is approached.

Although, ideally, the solution found by the EA should be independent of it, the choice of a specific fitness function might also play an important role in the speed and efficiency of the algorithm. We experimented with different cost functions (variance reduction, correlation), finding indeed rather similar solution models. To obtain maximum variability in best-fitting models, i.e., to best differentiate solution models with relatively similar fit as we progressively refine our search, we chose to use as cost function the exponential of the variance reduction, or

$$\exp \left(1 - \frac{\sum_{i=1}^n (\delta g_{mod}^i - \delta g_{obs}^i)^2}{\sum_{i=1}^n (\delta g_{obs}^i)^2} \right), \quad (4)$$

where δg_{mod}^i and δg_{obs}^i are the modeled and observed gravity anomalies, respectively, at the point i of a grid covering the Earth’s surface. In a set of preliminary tests, we have verified that the cost-function as defined by Eq. (4) results in the most effective convergence. Other cost functions that we have experimented with, including correlation and variance reduction (without exponential) did not allow to discriminate between close minima, beyond a certain refinement level.

We define an initial population, consisting of 100 randomly generated viscosity profiles. In most of our runs of the EA, convergence is achieved after roughly 100–300 generations (Fig. 1a, filled circles). The choice of the mutation rate adjustment (differ-

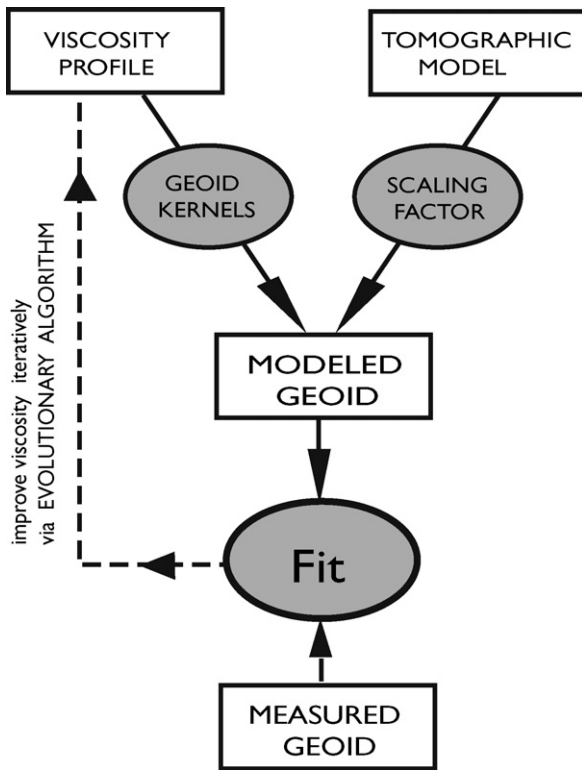


Fig. 2. After choosing velocity-to-density scaling relationship and tomographic model, we seek the mantle viscosity profile corresponding to the best fit of GRACE gravity data. Density anomalies and gravity data are related through sensitivity kernels, whose form in turn depends on the viscosity profile.

ential fitness) is reflected by the trend of empty circles in Fig. 1a, representing the average fitness of the population for each generation: average fitness achieves a maximum at 10–20 generations, then decreases with increasing fitness of the best solution.

We set the total number of generations to 500, corresponding to 50,000 forward computations total; completing this task takes about 48 h on a dual 2.7 GHz PowerPC. Performance depends on the number of free parameters in the inverse problem (i.e. number of uniform viscosity layers), on the maximum considered harmonic degree, and on the precision chosen for the variables. Since gravity data have little sensitivity to changes in viscosity larger than three orders of magnitude (King, 1995), we used single precision (4 bytes) floating points variables, allowing approximately 7 digits of accuracy.

Fig. 2 illustrates the sequence of steps in our algorithm: at each generation, tomographic anomalies are translated into ρ anomalies, which are then used to compute the gravity field at the Earth's surface associated with each viscosity profile in the population. The best-fitting viscosity profiles are then combined by the EA to identify a new, more fit population (a new generation), and the whole procedure is iterated.

3. Analyses of the method's resolution and stability

3.1. Recovering a theoretical viscosity model

A major problem with deriving mantle viscosity from gravity observations is the non-uniqueness of the solution. According to Peltier (1998), robust conclusions cannot be derived only on the basis of the long wavelength component of the geoid, and additional data are needed to better constrain the inversion. In a similar analysis, King (1995) found that families of viscosity profiles with both high and low viscosity in the transition zone explain the observed

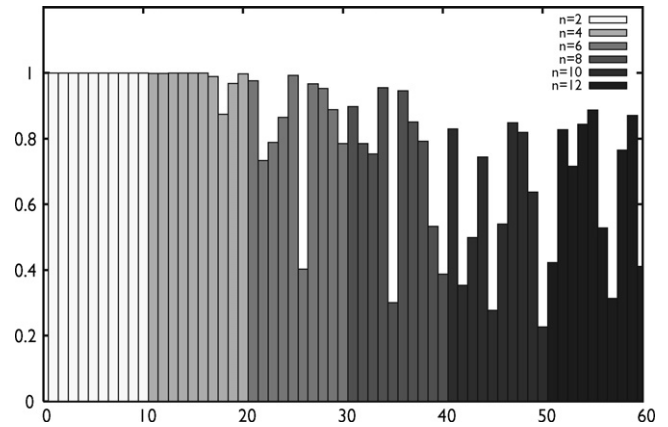


Fig. 3. Correlation between output and input model (maximum is 1) for the 60 synthetic tests conducted (10 for each value on the number n of uniform viscosity layers).

geoid equally well, and concluded that gravity measurements alone cannot distinguish between these different features. We reevaluate those inferences, conducting a number of synthetic experiments to estimate the radial resolution of our inversion. It is particularly important to determine the number of uniform viscosity layers that can be reliably constrained, and the range of relative changes in viscosity that can be expected.

We scale the v_S model S2ORTS (Ritsema et al., 1999, 2004) as illustrated in Fig. 8b (solid line). The scaling factor was obtained by inverting GRACE gravity data and S2ORTS tomographic model with an input viscosity profile taken from Mitrović and Forte (1997). The scaling factor $\zeta(r)$ is positive throughout the mantle, except for transition zones, where velocity anomalies are mainly compositional in origin. A thermal origin of anomalies, in fact, requires ζ to be positive, as, for any fixed composition, a perturbation in temperature causes perturbations of equal sign in density and v_S .

We randomly generate an 'input' profile of mantle viscosity, and use our mantle flow model to predict the corresponding gravity anomaly map. We then use the resulting, 'synthetic' gravity anomaly map as the database to be inverted via the EA. The correlation between output and input model, shown in Fig. 3 for 60 independent synthetic tests, is a measure of the accuracy and resolution of our method. We conducted 10 synthetic tests with 2-layer viscosity models, 10 with 4-layer models, and so on with 6-, 8-, 10- and 12-layer models. Fig. 3 shows that the non-uniqueness of the problem grows quickly with the number of inversion parameters. If the unknown viscosity profile is parameterized in terms of more than 5 uniform layers, the chance of converging to a wrong solution is high.

3.2. Testing the effects of different parameterization strategies and evolutionary regimes

We next replace synthetic data with true, free-air gravity anomalies from global Earth gravity model GGM02 (Tapley et al., 2005), based on the analysis of 363 days of GRACE (gravity recovery and climate experiment) in-flight data. Harmonic coefficients up to degree 160 are available, but we only consider degrees ≤ 8 , consistently with our decomposition of the tomographic models. We use the EA, as described above, to identify the best-fitting 5-layer model of relative changes in mantle viscosity, and, again, scale tomography model S2ORTS to define an a priori density map.

We first explore the influence of the population size, the number of generations and the seed used to initialize the EA on the inversion results. Fig. 4a shows the best-fitting viscosity profiles derived from runs of the EA with population sizes of 10, 50 and 100 indi-

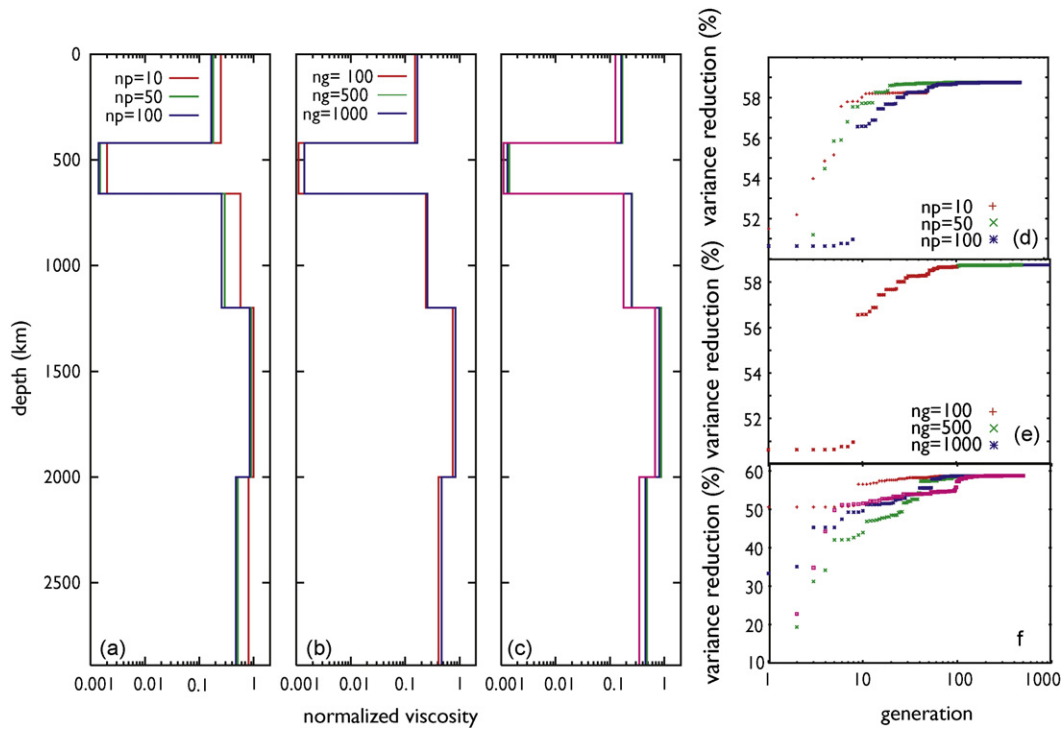


Fig. 4. Best-fitting viscosity profiles from runs (starting model: S20RTS) with different population size (a), number of generations (b), and initial seed (c). Only relative variations can be inferred from these models, that are normalized to the value of viscosity of the shallowest layer. Fit (variance reduction) of best model as a function of generation number, from inversions a, b, and c (e,d, and f, respectively).

viduals, evolved for 500 generations. Due to its stochastic nature, different runs of the EA inversion yield slightly varying results, but the important features (2-orders of magnitude viscosity jump at 410 km; smaller but significant jump at 1200 km) remain stable. Running the EA with 100 individuals for 100, 500 and 1000 generations, we obtain almost identical viscosity profiles (Fig. 4b). Inverting the same data with same population size and number of generations, but different seed, we find approximately the same radial viscosity profile (Fig. 4c). In all these cases, variance reduction (Fig. 4d–f) converges to approximately the same maximum.

We invert, again, gravity anomalies from GRACE starting from ν_5 model S20RTS and assuming a density-to-velocity scaling as in Fig. 8b (solid line). We repeat the experiment varying the number of constant-viscosity layers from 2 to 12. The resulting viscosity pro-

files, shown in Fig. 5, closely resemble the ones found in the other inversions of this Section, characterized by relatively low viscosity at depths corresponding to the mantle transition zone. Concerning the fitness to the data, the gravity anomalies computed in five out of the six cases reduce the variance of about 45–50%. Conversely, we found no 2-layer model that reduces the variance at all. We infer that at least two viscosity discontinuities in the mantle are required to explain the gravity data in consideration, and 2-layer models can be rejected a-priori.

We run the EA with several different parameterizations, characterized by the same total number (5), but different depth ranges, of uniform viscosity layers. We show the results in Fig. 6. Independently of parameterization, solutions tend to be characterized by low viscosity in the second shallowest layer, and/or transition

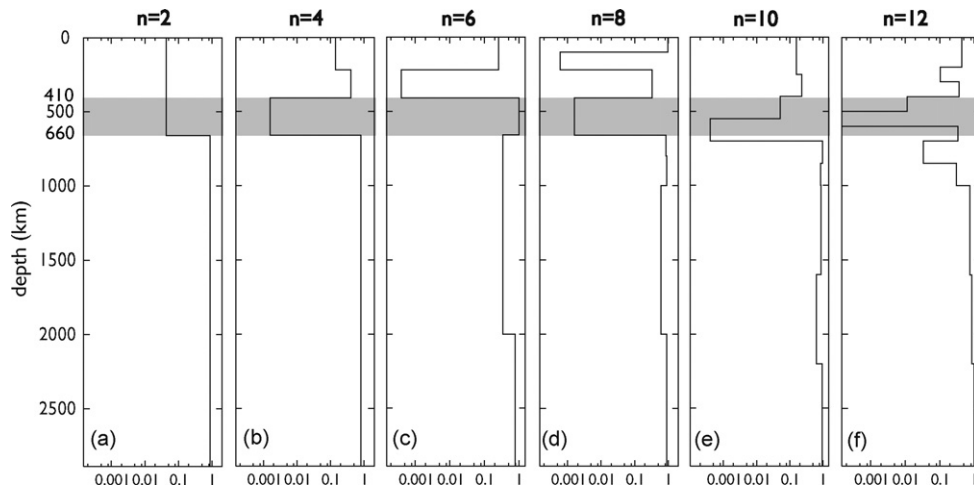


Fig. 5. Best-fitting mantle viscosity models resulting from inversions of GRACE free-air gravity anomalies and ν_5 models S20RTS with different number of layers n . Only relative variations can be inferred from these models.

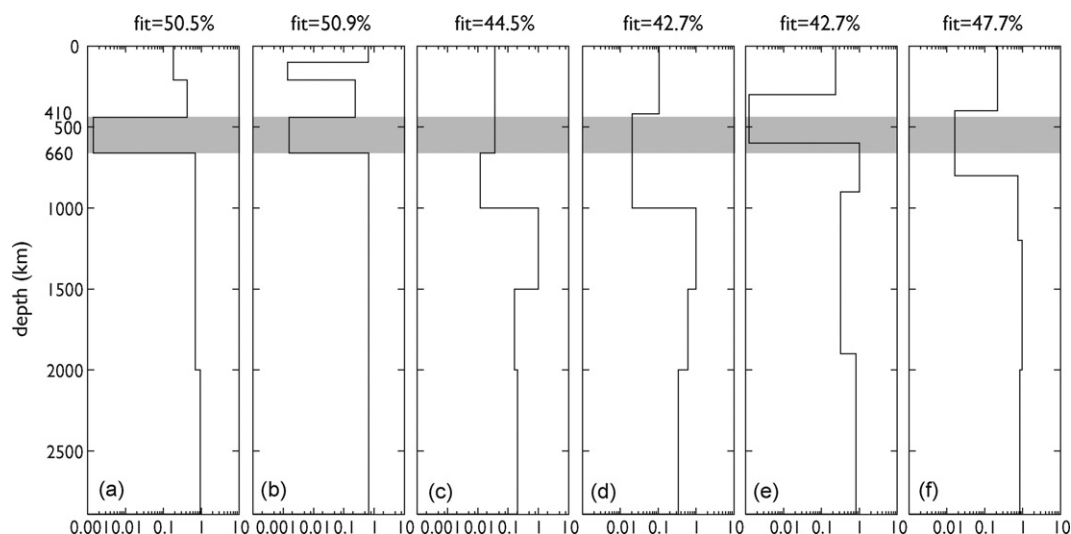


Fig. 6. Best-fitting mantle viscosity models resulting from inversions of GRACE free-air gravity anomalies and v_s model S20RTS, with same number of layers and different depths of viscosity discontinuities. Only relative variations can be inferred from these models. The fitness of gravity anomalies computed from these viscosity profiles to the data is displayed above each panel.

zone. The jump in viscosity found between 410 and 660 km depth ranges between 1 and 3 orders of magnitude. Variance reduction is maximum for the profiles in Fig. 6a and b, suggesting that a radial viscosity structure with finer parameterization in the upper mantle is more consistent with the observed gravity field.

3.3. Effect of the short-wavelength component of tomography

The neglect of harmonic degrees ≥ 8 is justified by the goal of identifying a whole-mantle viscosity profile, while relatively high harmonic degrees are mostly, if not only, sensitive to the upper mantle. We test, however, the possibility that the whole-mantle viscosity profile we find be perturbed by accounting for degrees >8 . We repeat the exercise described in Section 3.2, assuming a degree-16 density model scaled from the v_s model SMEAN (Becker and Boschi, 2002), and parameterizing mantle viscosity in terms of 5 uniform layers. The scaling factor coincides with the solid line in Fig. 8b. The result of this experiment is illustrated in Fig. 7. The variance reduction of gravity data (degrees 0 through 16) achieved by the SMEAN-based viscosity profile of Fig. 7 amounts to 45.7% and is therefore comparable to values found from the previous inversions. Most importantly, the viscosity profile we find is similar to most of the ones discussed above. Given its higher computational cost, we decide to drop the inversion of the high-degree component of gravity data.

4. Viscosity profiles resulting from different a priori assumptions on the Earth's density structure

4.1. Viscosity from inversion of gravity data and seismic velocity models

The most recent models of mantle rheology based on long-wavelength geoid data (Ricard and Wuming, 1991; King, 1995; Cadek et al., 1998; Mitrova and Forte, 2004) are defined in terms of 11–15 uniform-viscosity layers. We have shown in the previous section that our solution becomes increasingly non-unique for increasing number of uniform-viscosity layers, with the high chance of converging to a “wrong” minimum already with a 6-layer parameterization. We therefore restrict ourselves to 5-layer models consisting of an upper mantle extending from the Earth's surface down to the 660 km seismic discontinuity, and divided into two

layers at 410 km depth, and a lower mantle with possible viscosity discontinuities at 1200 and 2000 km. This radial parameterization is consistent with the most important boundaries given by King (1995), with Bullen's (1947) definition of the transition zone as a diffuse region of high seismic wave speed gradient extending from 400 to 1000 km, and with the results of Kawakatsu and Niu (1994) suggesting the presence of a seismic discontinuity at 920 km depth. The 2000 km discontinuity is based on Kellogg et al.'s (1999), van der Hilst and Karason's (1999) and Anderson's (2002) indications that the lowermost mantle, from a depth of ~ 1700 km down, never mixes with the rest of the mantle, forming a separate regime, with a boundary dividing layers with different composition.

So far we computed the surface gravity perturbations on the basis of the 3D density distribution constructed from the seismic tomographic model S20RTS. To measure how strongly our results are affected by the properties of the selected a-priori tomographic model, we repeat the experiment on the basis of different models, i.e. deriving density via $\zeta(r)$ from v_s models TRP246 (Trampert et al., 2004), and SPRD6 (Ishii and Tromp, 1999). TRP246 and SPRD6 also include ρ models, that we shall treat in Section 4.3.

Ishii and Tromp (1999) determined mantle S and P velocity and density structure, in addition to dynamic topography on the free surface and topography on the 660-km discontinuity and CMB, up to harmonic degree 6, from a combination of gravity and normal-mode splitting measurements. Trampert et al. (2004) used normal-mode splitting functions and surface-wave data to derive likelihoods of bulk sound and shear wave speed, density, and boundary topography. The seismic likelihoods are a complete and compact representation (mean and standard deviation) of all long-period seismic data, compatible with the observed gravity field, and are described by a linear combination of degree-2, -4, and -6 spherical harmonics.

We convert v_s anomalies to ρ heterogeneities using various scaling factors (Fig. 8b), calculated from various tomographic models and an input viscosity profile selected from Mitrova and Forte (1997). The three mantle viscosity profiles resulting, after running the EA, from the different tomographic models and scaling factors are shown in Fig. 8a. All profiles have approximately the same depth dependence, with important viscosity jumps at 410 and 660 km depth. For each run of the EA, corresponding to a certain tomography/density model, we also visualize in Fig. 8c–e the spread of the population, computing the mean and standard deviation of all

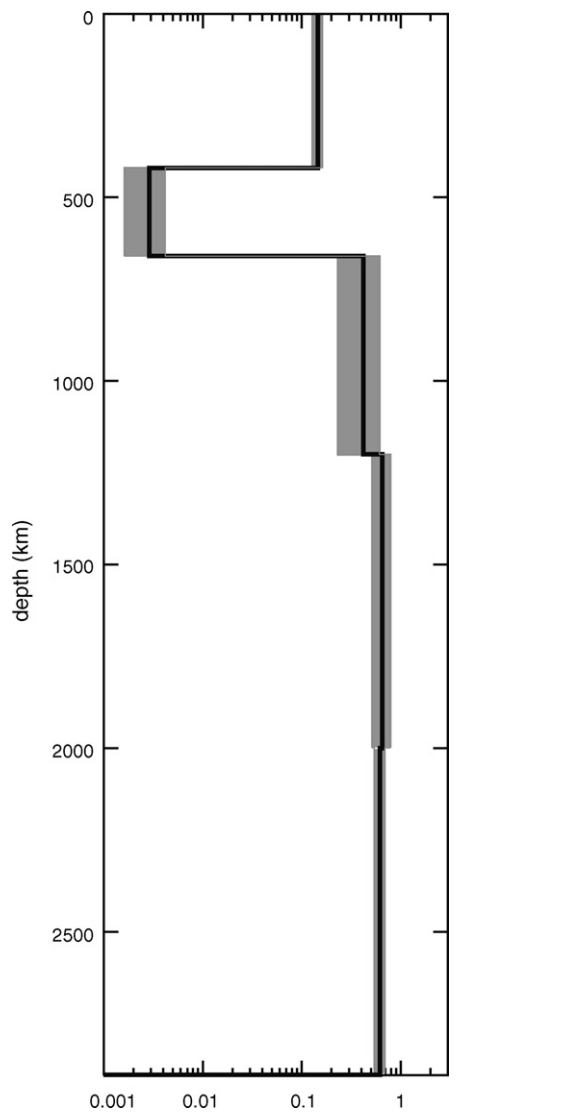


Fig. 7. Mantle viscosity profile obtained on the basis of SMEAN v_S model, assuming $n = 5$ and converting v_S anomalies to ρ anomalies via the scaling factors in Fig. (8b), solid line. The harmonics are summed up to degree $l = 16$. The figure shows average viscosity (in black) and standard deviation (gray intervals) of models with fit better than a given threshold.

viscosity profiles with fit above 53% (S20RTS); 40% (TRP246); 54% (SPRD6) (standard deviations are represented by gray intervals). The three thresholds have been chosen to always correspond to $\sim 10,000$ solution profiles. In all three cases, the best-fitting profiles are all very similar to each other, and different families of viscosity profiles fit the data equally well.

Fig. 9 shows viscosity profiles averaged over models that fit the data best than a prescribed value (30, 40 and 50% in plots a, b, and c, respectively). All the profiles refer to the inversions of gravity data with the (scaled) tomographic model S20RTS. Even models with relatively low fit include a low-viscosity transition zone. Assuming that the EA samples the solution space sufficiently well, we infer that this feature is robust.

Our approach is contingent on the simplistic assumption that velocity and density be correlated (e.g. Karato, 1993; Deschamps et al., 2001). We test how different choices of values for the corresponding scaling factor affect our results. Fig. 10 f–j shows the scaling factors we assumed, accompanied by the corresponding solution models (Fig. 10a–e). Despite slight discrepancies in the viscosity of the shallow layers, the most remarkable feature, a narrow

low-viscosity zone located between the 410-km and the 660-km discontinuities, is seen in all of the five cases we considered. A low-viscosity layer in the transition zone was also found in independent analyses of the global geoid (King, 1995; King and Masters, 1992; Forte et al., 1993; Panasyuk, 1998), of post-glacial rebound (Milne et al., 1997) and of polar motion (Steinberger and O’Connell, 1997). Fewer authors found evidence that viscosity in the same region might be anomalously high (Ricard et al., 1989; Spada et al., 1991; King, 1995).

4.2. Assumptions on the scaling factor

Since the choice of the velocity-to-density scaling factor may impart a bias to our results, and since the ones used here do not incorporate any mineral physics constraints, we try to use alternative scalings such as the ones based on laboratory experiments (Karato and Karki, 2001; Cammarano et al., 2003). Given that mineralogy-derived scalings between velocity and density are still subjected to a lot of uncertainties, we invert the gravity data (degrees 1 through 8) with v_S velocity model SMEAN (Becker and Boschi, 2002) and a scaling taken from Simmons et al. (2007) (see Fig. 11 a, solid line), selected among the ones proposed by Karato and Karki (2001) on the basis of the fit to a set of combined seismic and convection-related observables. The resulting viscosity profile is displayed in Fig. 11b and does not differ significantly from the ones obtained with classical scalings, confirming the robustness of our results. The gravity anomalies computed with this viscosity achieve a variance reduction of 47.7%.

We then attempt to account for the difference between sub-continental and sub-oceanic mantle, revealed by seismic tomography some 40 years ago (Jordan, 1975). The high-velocity roots below continents, absent below oceans (see Romanowicz, 2003, for a review), are balanced by differences in the respective chemical composition. Here, we have computed radial models of ζ for oceans and continents separately. To define oceanic and continental areas, we have constructed a continent-ocean function derived from the 3SMAC tectonic regionalization (Nataf and Ricard, 1996). The sub-continental and sub-oceanic scaling factors (dashed and dotted lines in Fig. 11a) are significantly different at depths shallower than 260 km, with the continental one negative at depths up to 80 km. Again we invert gravity data up to degree 8 based on v_S velocity model, to find the viscosity profile of Fig. 11c, with variance reduction of 46.5%. This result confirms our earlier findings (Fig. 11b).

4.3. Viscosity from inversion of gravity data and density models

Albeit commonly used (Forte and Perry, 2000; Deschamps et al., 2002), the procedure of estimating Earth’s density via a depth-dependent scaling factor applied to seismic velocity models is, at least to some extent, inaccurate: lateral ρ anomalies directly observed from, e.g., normal-mode data are both uncorrelated with (Resovsky and Trampert, 2003), and too large with respect to (Ishii and Tromp, 1999; Trampert et al., 2004) seismic anomalies, for the scaling-factor approach to be valid. We replace the v_S velocity models used so far with the ρ models provided by Trampert et al. (2004) and Ishii and Tromp (1999), and determined from observations of the Earth’s free oscillations, which, unlike travel-time or waveform data, are directly sensitive to density. Several authors (Resovsky and Ritzwoller, 1999; Romanowicz, 2001; Kuo and Romanowicz, 2002) objected that density cannot yet be constrained in this way, because the sensitivity kernels for density are much smaller than those for velocities, and because the least-squares inversions conducted in this kind of studies require the use of a starting model, the choice of which is critical for the reliability of the results.

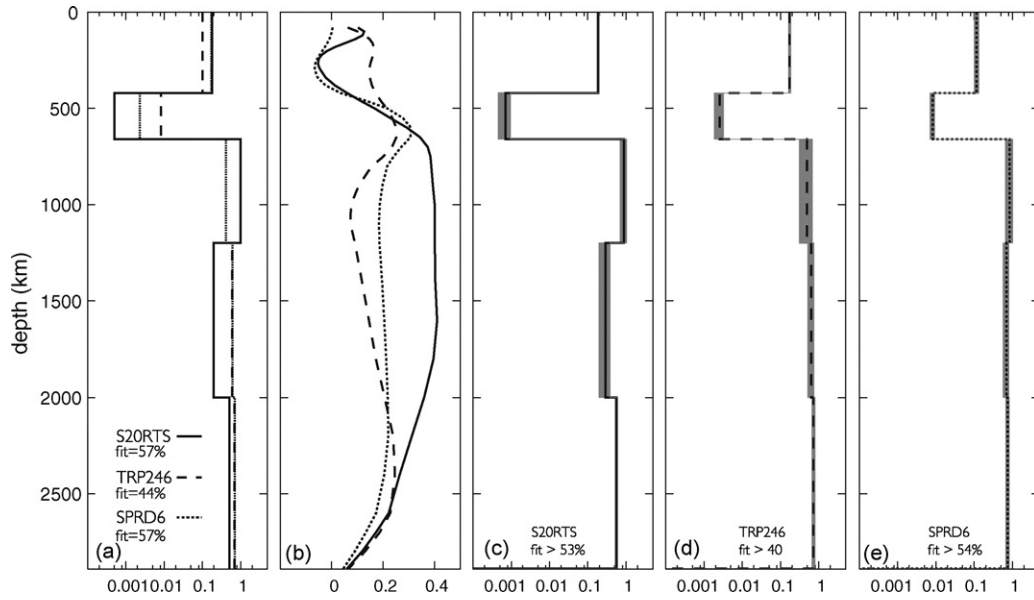


Fig. 8. Best-fitting viscosity profile (a) obtained on the basis of some v_s models, assuming $n = 5$ and converting v_s anomalies to ρ anomalies via the scaling factors in (b). Frames (c–e) show average viscosity (black lines) and standard deviation (gray intervals) of models with fit better than a given threshold.

In Fig. 12 we compare the best viscosity profiles found via EA on the basis of the ρ models, with those resulting from the corresponding v_s models TRP246 and SPRD6. The difference with the profiles derived from velocity models (plotted for comparison in Fig. 12a), is striking: viscosity increases almost monotonically with depth for the profile corresponding to ρ model TRP246, and the low-viscosity transition zone that characterizes all our solution viscosity models becomes much less pronounced in the profile derived from ρ model SPRD6. It is remarkable that variance reduction achieved by density with respect to velocity models drops from 57% to 10% for SPRD6 and becomes negative for TRP246, even though low even degrees of gravity data are appropriately fit by Ishii and Tromp (1999). We explain this discrepancy in terms of the different approach used here with respect to the studies of Trampert et al. (2004) and Ishii and Tromp (1999), to establish a relationship between mantle flow and observations of gravity. We account for mantle flow explicitly

(e.g., Richards and Hager, 1984), while those authors do it by allowing for deflections of the internal boundaries. In the past, it has been assumed that the two approaches are equivalent, but we believe that this assumption must be reevaluated. We show in Fig. 13 how gravity anomalies computed on the basis of viscosity profiles from Fig. 12 compare to GRACE data. While the v_s -based viscosity profile of Fig. 13a reproduces the data relatively well, the ρ -based results are in fact completely off.

An alternative density model has been derived by Simmons et al. (2007), based upon seismic travel-time data, and geodynamic observations including dynamic topography, gravity, plate motions and CMB ellipticity. Simmons et al.'s (2007) approach also implicitly accounts for both thermal and compositional buoyancy effects on mantle flow. We have repeated our inversion experiment assuming density structure as mapped by Simmons et al. (2007). The resulting viscosity profile, shown in Fig. 14, confirms the presence of a

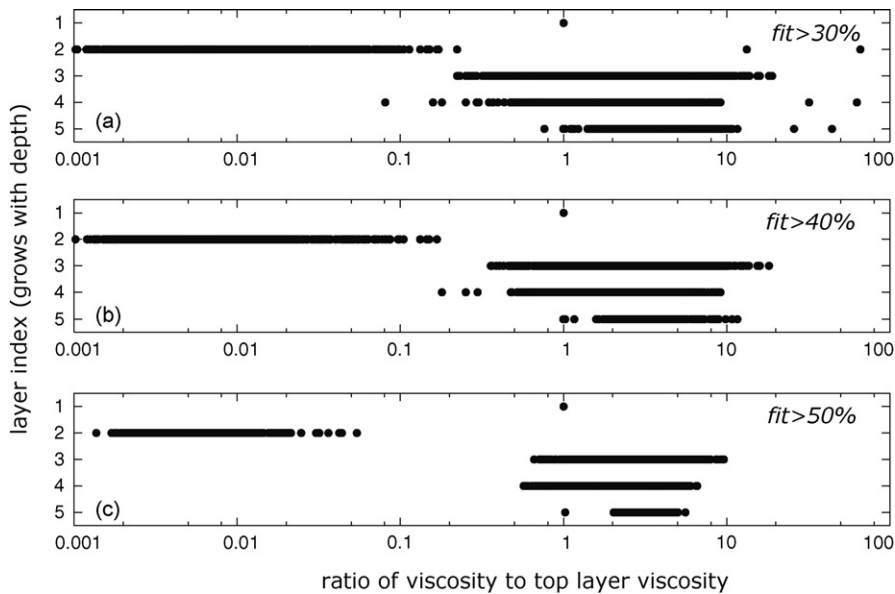


Fig. 9. Range of variability of the viscosity of the 5 layers (normalized to the value of viscosity of the shallowest layer) obtained inverting gravity data with density structure from v_s model S20RTS.

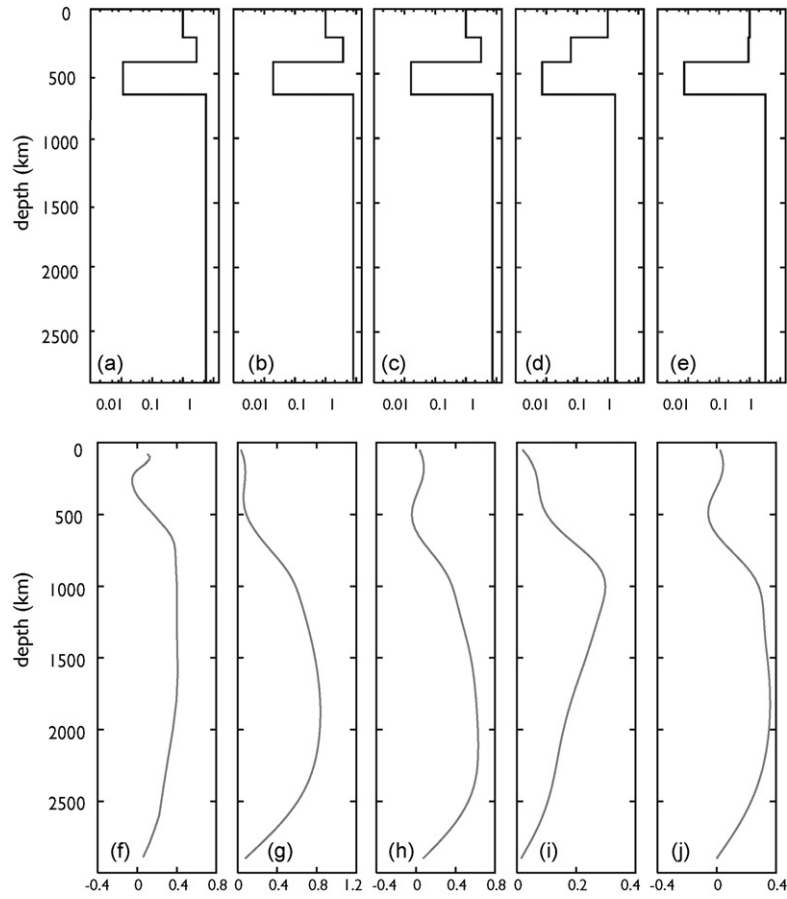


Fig. 10. Mantle viscosity models (a–e) from inversion of GRACE data and ν_s model S20RTS with different velocity-to-density scaling factors (f–j). The scalings employed are derived by inverting gravity data on the basis of different tomographic models.

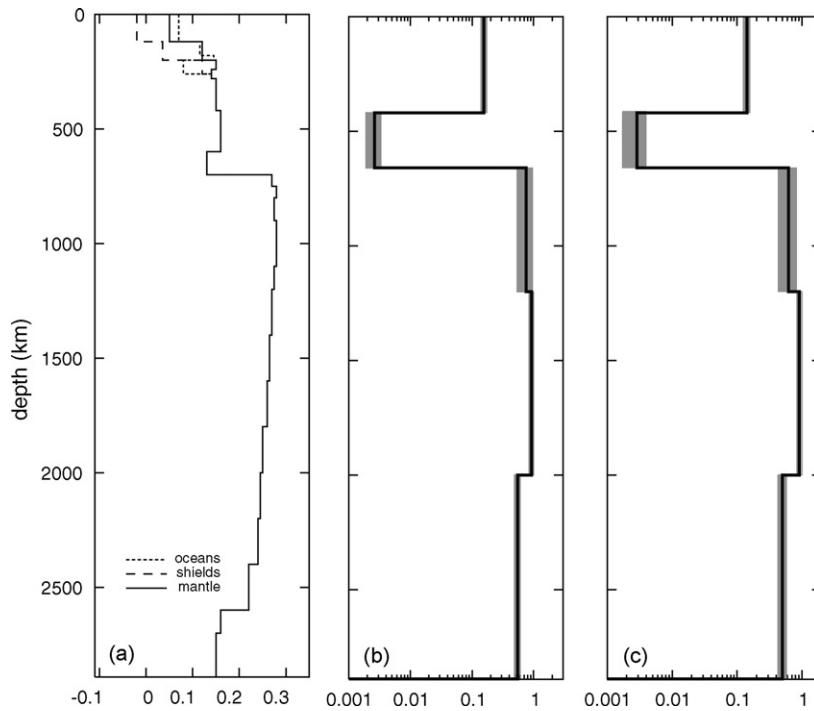


Fig. 11. Viscosity profile (b) obtained on the basis of SMEAN ν_s model, assuming $n = 5$ and converting ν_s anomalies to ρ anomalies via the scaling factor in (a), solid line (Karato and Karki, 2001). Frame (c) shows average viscosity derived using different velocity-to-density scaling factors for suboceanic mantle (dotted line) and subcontinental mantle (dashed line). Gray intervals represent the standard deviation of models with fit better than a given threshold.

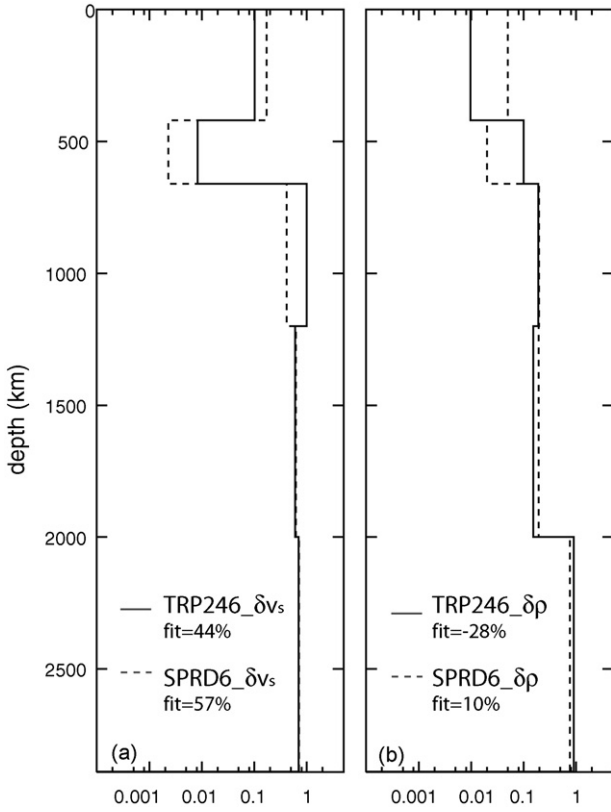


Fig. 12. Best-fitting viscosity profiles based on ν_s models (panel a) TRP246 (solid line) and SPRD6 (dashed line) and ρ models (panel b) TRP246 (solid line) and SPRD6 (dashed line).

low-viscosity zone in the upper-to-lower mantle transition zone. It differs from those of the previous sections in the lower mantle, where it is characterized by lower values of relative viscosity, and by a pronounced viscosity jump at 2000 km depth. The corresponding variance reduction of the inverted gravity data amounts to 87%, much higher than achieved in earlier inversions.

5. CMB topography

Undulations of the CMB are generally believed to be the result of radial stresses generated by convective mantle flow induced, in turn, by lateral variations in density throughout the mantle. We compute here the topography of the CMB from the same ν_s and ρ models as in Section 4.

The spherical harmonic coefficients δb_l^m of flow-induced CMB topography are related to density perturbations $\delta \rho_l^m$ by topography kernels B_l via an equation similar to (1),

$$\delta b_l^m(\theta, \phi) = \frac{1}{\Delta \rho_{cm}} \int B_l(\nu/\nu_0, r) \delta \rho_l^m(r, \theta, \phi) dr \quad (5)$$

(Forte et al., 1995), where $\Delta \rho_{cm} = -4.43 \text{ Mg m}^{-3}$ is the density jump across the CMB according to PREM (Dziewonski and Anderson, 1981), and the integration is done from the radius of the CMB to the Earth's surface. The topography kernels B_l are calculated, as for the gravity anomalies, in the degree range $l = 2\text{--}8$ and, like geoid kernels, they implicitly depend on the (relative) viscosity profile of the mantle (ν/ν_0). As before, the harmonic coefficients $\delta \rho_l^m$ are found from a scaled velocity model.

We show in Fig. 15 the total CMB topography obtained from ν_s models S20RTS, TRP246, SPRD6 (Fig. 15a–c), and that obtained from ρ models TRP246 and SPRD6 (Fig. 15d and e). The viscosity profiles

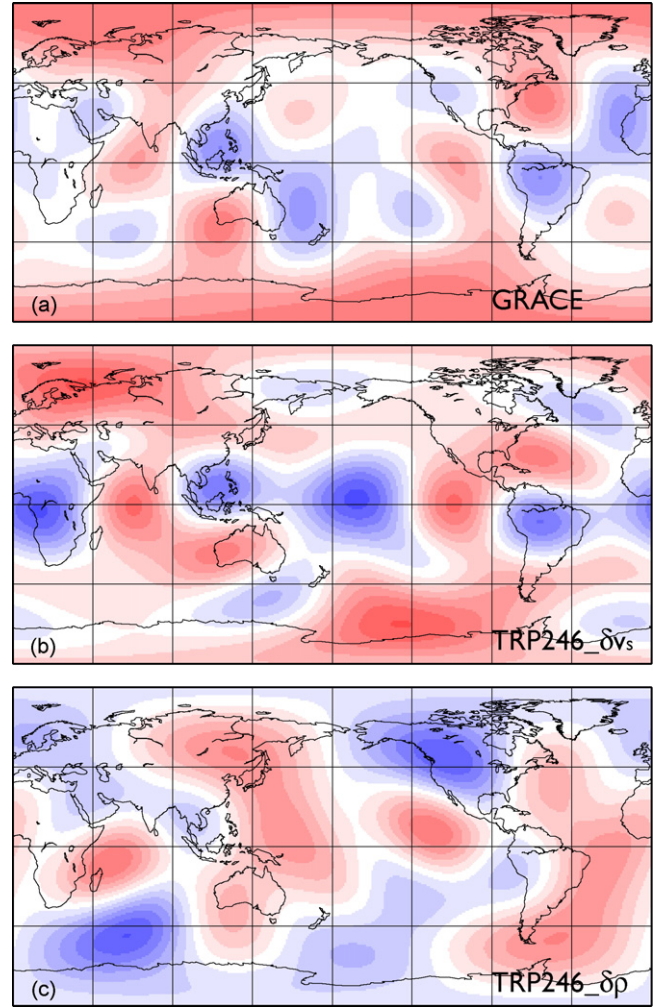


Fig. 13. Map of free-air gravity anomalies retrieved by GRACE campaign (panel a), computed on the basis of tomographic ν_s model TRP246 (panel b) and computed on the basis of TRP246 ρ model (panel c). The scale for each map is $\pm 40 \text{ mGal}$ (a), $\pm 20 \text{ mGal}$ (b,c). Blue colors indicate regions of higher than average gravity, and red colors indicate regions of lower than average gravity.

implemented correspond, for each ν_s or ρ model, to the best-fitting profiles found in Sections 3 and 4 inverting that same model.

The ν_s -derived topographies are in close agreement with most published results (Morelli and Dziewonski, 1987; Forte et al., 1995; Obayashi and Fukao, 1997), characterized by a ring of depressions over the Americas, Eastern Asia, and Australia. CMB deflections based on ν_s model SPRD6 compares well with those found by Forte et al. (1995), but differ slightly in amplitude. Maps of CMB topography computed directly from ρ models display a more complex pattern, and have amplitude three times bigger, though very similar to each other both in shape and in amplitude. Again, differences between the topography predicted by ν_s and ρ result from the fact that the two distribution are not correlated (e.g., Trampert et al., 2004).

The dynamic topography at the CMB is not directly observable from surface data, with the exception of the component δb_2^0 of the CMB topography, called excess or dynamic ellipticity, which can be inferred via VLBI measurements of the period of the Earth's free-core nutation. The most recent inferences (Mathews et al., 2002, 1999) suggest a value closer to 0.4 km, rather than 0.5 km as determined in the earlier study by Gwinn et al. (1986). The values of δb_2^0 we obtain (Table 1) on the basis of the different ν_s and ρ models are about three times larger, having absolute value bigger than

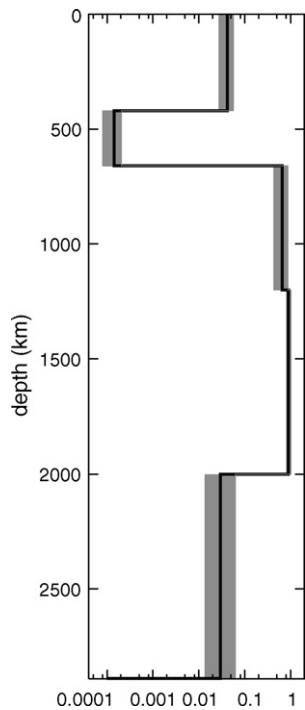


Fig. 14. Viscosity profile (b) obtained on the basis of the ρ model by Simmons et al. (2007). The black line represents the average viscosity, gray intervals correspond the standard deviation of models with fit better than a given threshold.

1.5 km. The poor fit to the observations of CMB ellipticity may be justified by the fact that our mantle flow models are constrained to only fit the free-air gravity data; other potential reasons are a poor velocity-to-density scaling in the lower mantle and a poorly resolved viscosity at depth.

Table 1

Predicted excess CMB topography (km) obtained from some ν_s and ρ models.

Model	Type of anomaly	Dynamic ellipticity (km)
SORTS	$\delta\nu_s$	1.5
TRP246	$\delta\nu_s$	1.8
SPRD6	$\delta\nu_s$	1.8
TRP246	$\delta\rho$	4.8
SPRD6	$\delta\rho$	1.5

6. Discussion and conclusions

We have applied the evolutionary algorithm technique to identify a spherically symmetric model of viscosity in the Earth's mantle from global observations of free-air gravity anomalies in the degree range $l = 2-8$. We modeled perturbations in the Earth's gravity field induced by density heterogeneities via a viscous flow model, with no a priori barrier for the vertical flux at the 660 km discontinuity. This approach allows to derive the depth-dependence of relative viscosity, constraining its value uniquely in up to five uniform layers. The solutions we obtain on the basis of ν_s models S2ORTS or SMEAN are consistent with classical estimates of the upper-to-lower-mantle viscosity jump. Additionally, they are characterized by a transition zone less viscous than the uppermost mantle by 2 or 3 orders of magnitude. This feature is parameterization-independent, and is shared by the viscosity profile we find based on the density model of Simmons et al. (2007).

The found softening of transition zone minerals could be related to various processes: (i) high content of water (van der Meijde et al., 2003; Huang et al., 2005; Bolfan-Casanova, 2005); (ii) phase changes that occur at these depths, like transformation of pyroxenes into garnet, or olivine successively into wadsleyite and into ringwoodite; (iii) the extreme softening of a material as it undergoes a phase transition, known as transformational superplasticity (Sammis and Dein, 1974).

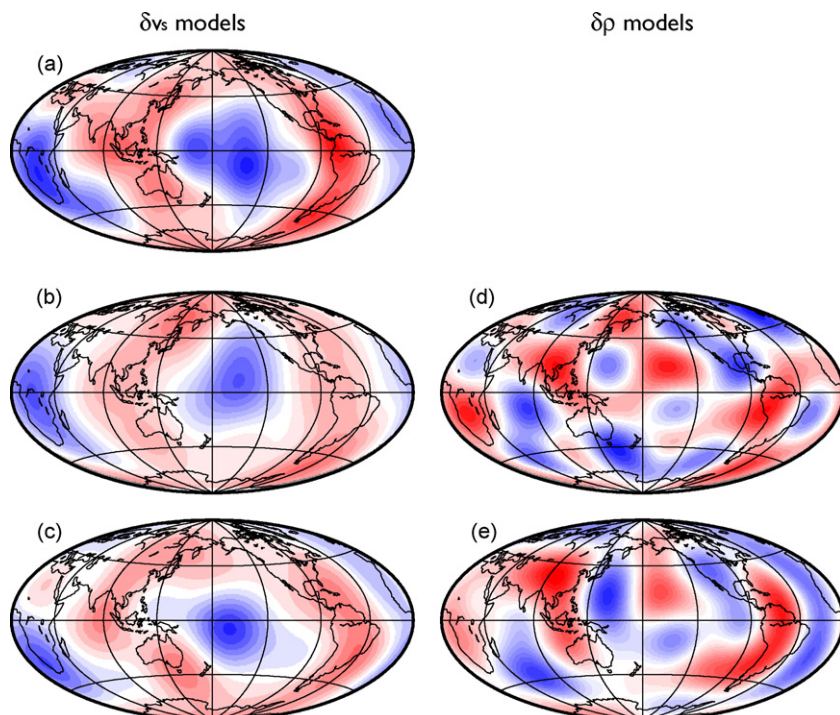


Fig. 15. CMB dynamic topography based on ν_s models S2ORTS, TRP246, SPRD6 (frames a–c, respectively); and on ρ models TRP246 and SPRD6 (frames d and e). The scale for each map is ± 5 km (a and b), ± 8 km (c), ± 15 km (d), ± 12 km (e). Blue colors indicate elevation, red colors indicate depression.

- (i) Several high-pressure mineral-physics studies (Smyth, 1987; Kawamoto et al., 1996; Kohlstedt et al., 1996) have shown that transition zone minerals at average mantle temperatures have anomalously high water solubility compared to upper and lower mantle minerals, suggesting that the transition zone might act as a water reservoir. The potential presence of water in the transition zone, also revealed by the seismological analysis of van der Meijde et al. (2003), could also explain the discrepancy between the velocity jump at 410 km observed seismically and the one expected for an olivine-rich (pyrolite) mantle (Duffy and Anderson, 1989; Anderson, 1989; Anderson and Bass, 1986). Smyth and Jacobsen (2006) proposed that lateral velocity variations in the transition zone may reflect variations in hydration rather than variations in temperature. Despite the many evidences of significant amounts of water in the transition zone, the actual content of water is still poorly constrained, being estimated to range between 0.1 wt% and 3 wt% (Bercovici and Karato, 2003). Also, the effect of water on material properties is not clear, even if it is known that it controls the strength and deformation mechanism of minerals (Kavner, 2003) and thus the rheology of rocks (Karato, 1998). Since viscous deformation is a macroscopic form of creep depending on the presence of defects in the lattice structure, and since water increases the number of defects within a crystal, it enhances diffusion rates and this should decrease viscosity.
- (ii) The possible role of the dilution of pyroxenes into garnets (the major phase change at transition zone depths) could be enlightened by the knowledge of the creep laws for these two minerals. To date, available experimental data are sparse, but uniaxial compression and hot hardness tests (Karato et al., 1995) demonstrated that the resistance to plastic deformation in garnets is significantly higher than most of the other minerals in the Earth's mantle; the pyroxene-garnet phase change, then, cannot explain the low viscosity in the transition zone. An alternative explanation could reside in the transformation of olivine into wadsleyite and then ringwoodite (Artem Oganov, personal communication, 2007).
- (iii) The third possible explanation for the soft transition zone might be attributed to a phenomenon known as transformational superplasticity, first pointed out by Sammis and Dein (1974), that consists in a dramatic reduction in effective viscosity observed during a phase transition in materials like metals and ceramics (Poirier, 1985; Maehara and Langdon, 1990; Meike, 1993). Panasyuk and Hager (1998) tested a model of transformational superplasticity for the upper mantle and estimated the degree of softening for mantle material at the phase change at 400 km depth: the viscosity decrease would be of 1–2 orders of magnitude, consistent with what we found.

While anomalously low values of viscosity in the transition zone are a robust result, some of our findings cast doubts on certain aspects of the approach we followed. In particular, we have illustrated in Section 4.3 (Figs. 12 and 13) the disagreement between density-based and velocity-based modeling results. We have explained it as the consequence of a discrepancy between the approach followed here, where mantle flow is modeled explicitly (e.g., Richards and Hager, 1984), and that of, e.g., Ishii and Tromp (1999) and Trampert et al. (2004), who account for mantle flow implicitly, parameterizing the undulation of internal discontinuities (e.g., lower-upper-mantle boundary, core–mantle boundary). If any of these methods is to be implemented again in the future, the theoretical reasons for the discrepancy should be quantified. Here (end of Section 4.3) we show that our approach is consistent with that of Simmons et al. (2007), who mapped mantle density

from seismic travel-times and a suite of geodynamic data including gravity anomalies, and neglecting normal-mode observations.

In view of the continuing, fast growth of computational power, an alternative solution would possibly be that of resorting fully numerical formulations instead of analytical ones. Numerical approaches to the inverse problem have been made effective both in seismology (Tromp et al., 2005; Peter et al., 2007) and geodynamics (Bunge et al., 2003), via the application of ideas based on the adjoint method of Tarantola (1984).

Acknowledgments

This research was partially supported by the NERIES program. We are grateful to Adam Dziewonski and Giorgio Spada for fruitful discussions, to Dave Yuen for continuing encouragement, and to Miaki Ishii, Jeroen Ritsema and Jeannot Trampert for providing their tomographic models. We thank Rob Moucha and Mark Jelinek for useful comments that improved a first version of this paper. The implementation of the EA technique used in this analysis is made via the PIKAIA Fortran routine, developed by Charbonneau and Knapp (1995) at the High Altitude Observatory in Boulder, Colorado, and available electronically on the Observatory ftp archive. Figures were prepared with GMT by Wessel and Smith (1991).

References

- Anderson, D.L., Bass, J.D., 1986. Transition region of the Earth's upper mantle. *Nature* 320, 321–328.
- Anderson, D.L., 1989. *Theory of the Earth*. Blackwell, Boston.
- Anderson, D.L., 2002. The case for irreversible chemical stratification of the mantle. *Int. Geol. Rev.* 44, 97–116.
- Becker, T.W., Boschi, L., 2002. A comparison of tomographic and geodynamic mantle models. *Geochem. Geophys. Geosyst.* 3, 2001GC000168.
- Bercovici, D., Karato, S., 2003. Whole-mantle convection and the transition-zone water filter. *Nature* 438, 39–44.
- Bolfan-Casanova, N., 2005. Water in the Earth's mantle. *Miner. Mag.* 69, 229–257.
- Boschi, L., Becker, T.W., Steinberger, B., 2007. Mantle plumes: dynamic models and seismic images. *Geochem. Geophys. Geosyst.* 8, Q10006, doi:10.1029/2007GC001733.
- Bullen, K.E., 1947. *An Introduction to the Theory of Seismology*. Cambridge University Press, Cambridge.
- Bunge, H.P., Hagelberg, C.R., Travis, B.J., 2003. Mantle circulation models with variational data assimilation: inferring past mantle flow and structure from plate motion histories and seismic tomography. *Geophys. J. Int.* 152 (2), 280–301, doi:10.1046/j.1365-246X.2003.01823.x.
- Cadek, O., Yuen, D.A., Cizkova, C., 1998. Mantle viscosity inferred from geoid and seismic tomography by genetic algorithms: results for layered mantle flow. *Phys. Earth Planet. Inter.* 107, 307–326.
- Cammarano, F., Goes, S., Vacher, P., Giardini, D., 2003. Inferring upper mantle temperatures from seismic velocities. *Phys. Earth Planet. Inter.* 138, 197–222.
- Charbonneau, P., Knapp, B., 1995. A User's guide to PIKAIA 1.0, NCAR Technical Note 418+IA. National Center for Atmospheric Research, Boulder.
- Corrieu, V., Thoraval, C., Ricard, Y., 1995. Mantle dynamics and geoid Green functions. *Geophys. J. Int.* 120 (2), 516–523.
- Dal Forno, G., Gasperini, P., Boschi, E., 2005. Linear or nonlinear rheology in the mantle: a 3D finite-element approach to postglacial rebound modeling. *J. Geodyn.* 39, 183–195.
- Deschamps, F., Snieder, R., Trampert, J., 2001. The relative density-to-shear velocity scaling in the uppermost mantle. *Phys. Earth Planet. Inter.* 124, 193–211.
- Deschamps, F., Trampert, J., Snieder, R., 2002. Anomalies of temperature and iron in the uppermost mantle inferred from gravity data and tomographic models. *Phys. Earth Planet. Inter.* 129, 245–264.
- Duffy, T.S., Anderson, D.L., 1912. Seismic velocities in mantle minerals and the mineralogy of the upper mantle. *J. Geophys. Res.* 94, 1895.
- Dziewonski, A.M., Anderson, D.L., 1981. Preliminary reference Earth model. *Phys. Earth Planet. Inter.* 25, 297–356.
- Forté, A.M., Peltier, W.R., 1987. Plate tectonics and aspherical Earth structure: the importance of poloidal–toroidal coupling. *J. Geophys. Res.* 92, 3645–3679.
- Forté, A.M., Peltier, W.R., 1991. Viscous flow models of global geophysical observables: 1. Forward problems. *J. Geophys. Res.* 96, 20131–20159.
- Forté, A.M., Dziewonski, A.M., Woodward, R.L., 1993. Aspherical structure of the mantle, tectonic plate motions, nonhydrostatic geoid and topography of the core–mantle boundary. In: Le Mouél, J.-L., Smylie, D.R., Herring, T. (Eds.), *Dynamics of Earth's Deep Interior and Earth Rotation*. Am. Geophys. Union, Washington, DC, pp. 135–166.
- Forté, A.M., Woodward, R.L., Dziewonski, A.M., 1994. Joint inversions of seismic and geodynamic data for models of three-dimensional mantle heterogeneity. *J. Geophys. Res.* 99, 21857–21877.

- Forte, A.M., Peltier, W.R., 1994. The kinematics and dynamics of poloidal-toroidal coupling in mantle flow: the importance of surface plates and lateral viscosity variations. *Adv. Geophys.* 36, 1–119.
- Forte, A.M., Mitrovica, J.X., Woodward, R.L., 1995. Seismic-geodynamic determination of the origin of excess ellipticity of the core-mantle boundary. *Geophys. Res. Lett.* 22, 1013–1016.
- Forte, A.M., Mitrovica, J.X., 1996. New inferences of mantle viscosity from joint inversion of long-wavelength mantle convection and post-glacial rebound data. *Geophys. Res. Lett.* 23, 1147–1150.
- Forte, A.M., Perry, H.K.C., 1940–1944. Geodynamic evidence for a chemically depleted continental tectosphere. *Science* 290 (5498), 1940–1944.
- Forte, A.M., Mitrovica, J.X., 2001. High Viscosity Deep Mantle Flow and Thermochemical Structure Inferred From Seismic and Geodynamic Data. *Nature* 410, 1049–1056.
- Gwinn, C.R., Herring, T.A., Shapiro, I.I., 1986. Geodesy by radio interferometry: studies of the forced nutations of the Earth. 2. Interpretation. *J. Geophys. Res.* 91, 4755–4765.
- Hager, B.H., O'Connell, R.J., 1981. A simple global model of plate dynamics and mantle convection. *J. Geophys. Res.* 86, 4843–4867.
- Hager, B.H., Richards, M.A., 1989. Long-wavelength variations in Earth's geoid: physical models and dynamical implications. *Philos. Trans. R. Soc. Lond. A* 328, 309–327.
- Haskell, N.A., 1935. The motion of a fluid under a surface load 1. *Physics* 6, 265–269.
- Huang, X., Yousheng, X., Karato, S., 2005. Water content in the transition zone from electrical conductivity of wadsleyite and ringwoodite. *Nature* 434 (7034), 746–749.
- Ishii, M., Tromp, J., 1999. Normal-mode and free-air gravity constraints on lateral variations in velocity and density of Earth's mantle. *Science* 285, 1231–1236.
- Jordan, T.H., 1975. The continental tectosphere. *Rev. Geophys. Space Phys.* 13, 112.
- Kaban, M.K., Rogozhina, I., Trubitsyn, V., 2007. Importance of lateral viscosity variations in the whole mantle for modelling of the dynamic geoid and surface velocities. *J. Geodyn.* 43, 262–273.
- Karato, S.-I., 1993. Importance of anelasticity in the interpretation of seismic tomography. *Geophys. Res. Lett.* 20, 1623–1626.
- Karato, S., Wang, Z.C., Liu, B., Fujino, K., 1995. Plastic deformation of garnets: systematics and implications for the rheology of the mantle transition zone. *Earth Planet. Sci. Lett.* 130 (1–4), 13–30.
- Karato, S.I., 1998. Plastic deformation of silicate spinel under transition-zone conditions of the Earth's mantle. *Nature* 395, 266–269.
- Karato, S., Karki, B.B., 2001. Origin of lateral heterogeneity of seismic wave velocities and density in the deep mantle. *J. Geophys. Res.* 106, 21, 771–21, 783.
- Kaufmann, G., Lambek, K., 2002. Glacial isostatic adjustment and the radial viscosity profile from inverse modeling. *J. Geophys. Res.* 107, ETG5–1–ETG5–15.
- Kaufmann, G., Wu, P., 2002. Glacial isostatic adjustment in fennoscandia with a three-dimensional viscosity structure as an inverse problem. *Earth Planet. Sci. Lett.* 197 (1–2), 1–10.
- Kavner, A., 2003. Elasticity and strength of hydrous ringwoodite at high pressure. *Earth Planet. Sci. Lett.* 214, 645–654.
- Kawakatsu, H., Niu, F., 1994. Seismic evidence for a 920-km discontinuity in the mantle. *Nature* 371, 301–305.
- Kawamoto, T., Hergig, R.L., Holloway, J.R., 1996. Experimental evidence for a hydrous transition zone in the early Earth's mantle. *Earth Planet. Sci. Lett.* 142, 587–592.
- Kellogg, L.H., Hager, B.H., van der Hilst, R.D., 1999. Compositional stratification in the deep mantle. *Science* 283, 1881–1884.
- Kido, M., Cadec, O., 1997. Inferences of viscosity from the oceanic geoid: Indication of a low viscosity zone below the 660-km discontinuity. *Earth Planet. Sci. Lett.* 151, 125–138.
- Kido, M., Yuen, D.A., Cadec, O., Nakakuki, T., 1998. Mantle viscosity derived by genetic algorithm using oceanic geoid and seismic tomography for whole-mantle versus blocked-flow situations. *Phys. Earth Planet. Inter.* 107, 307–326.
- King, S.D., Masters, G., 1992. An inversion for radial viscosity structure using seismic tomography. *Geophys. Res. Lett.* 19, 1551–1554.
- King, S.D., 1995. Radial models of mantle viscosity: results from a generic algorithm. *Geophys. J. Int.* 122, 725–734.
- Kohlstedt, D.L., Keppeler, H., Rubie, D.C., 1996. The solubility of water in alpha, beta and gamma phases of (Mg,Fe)₂SiO₄. *Contrib. Miner. Petrol.* 123, 345–357.
- Kuo, C., Romanowicz, B., 2002. On the resolution of density anomalies in the Earth's mantle using spectral fitting of normal mode data. *Geophys. J. Int.* 150, 162–179.
- Maehara, Y., Langdon, T.G., 1990. Superplasticity in ceramics. *J. Mater. Sci.* 25, 2275–2286.
- Mathews, P., Buffett, B.A., Herring, T.A., 1999. What do nutations tell us about the Earth's interior? *Eos Trans.* 80 (46), 19.
- Mathews, P.M., Herring, T.A., Buffett, B.A., 2002. Modeling of nutation and precession: new nutation series for nonrigid Earth and insights into the Earth's interior. *J. Geophys. Res.* 107, 10.1029/2001JB000390.
- Meike, A., 1993. A critical review of investigations into transformation plasticity. In: Boland, J.N., Fitz Gerald, J.D. (Eds.), *Defects and Processes in the Solid State: Geoscience Applications* (the McLaren volume). Elsevier, Developments in Petrology, p. 14.
- Milne, G.A., Mitrovica, J.X., Forte, A.M., 1997. The sensitivity of glacial isostatic adjustment predictions to a low-viscosity layer at the base of the upper mantle. *Earth Planet. Sci. Lett.* 154, 265–278.
- Mitrovica, J.X., Peltier, W.R., 1995. Constraints on mantle viscosity based upon post-glacial uplift data from the Hudson Bay region. *Geophys. J. Int.* 122, 353–377.
- Mitrovica, J.X., Forte, A.M., 1997. The radial profile of mantle viscosity: results from the joint inversion of convection and post-glacial rebound observables. *J. Geophys. Res.* 102, 2751–2769.
- Mitrovica, J.X., Forte, A.M., 2004. A new inference of mantle viscosity based upon joint inversion of convection and glacial isostatic adjustment data. *Earth Planet. Sci. Lett.* 225, 177–189.
- Morelli, A., Dziewonski, A. M., 1987. Topography of the core-mantle boundary and lateral homogeneity of the liquid core. *Nature* 325, 678–683, doi:10.1038/325678a0.
- Moucha, R., Forte, A.M., Mitrovica, J.X., Daradich, A., 2007. Lateral variations in mantle rheology: implications for convection related surface observables and inferred viscosity models. *Geophys. J. Int.* 169 (1), 113–135.
- Nataf, H.C., Ricard, Y., 1996. 3SMAC: an a priori tomographic model for upper mantle based on geophysical modeling. *Phys. Earth Planet. Inter.* 95, 101–122.
- Obayashi, M., Fukao, Y., 1997. P and PcP travel time tomography for the core-mantle boundary. *J. Geophys. Res.* 102, 17, 825–17, 841.
- Panasuyuk, S.V., Hager, B.H., Forte, A.M., 1996. Understanding the effects of mantle compressibility on geoid kernels. *Geophys. J. Int.* 124, 121–133.
- Panasuyuk, S.V., 1998. The effect of compressibility, phase transformations, and assumed density structure on mantle viscosity inferred from Earth's gravity. Ph.D. Thesis, Massachusetts Institute of Technology.
- Panasuyuk, S.V., Hager, B.H., 1998. A model of transformational superplasticity of the upper mantle. *Geophys. J. Int.* 133, 741–755.
- Panasuyuk, S.V., Hager, B.H., 2000. Models of isostatic and dynamic topography, geoid anomalies, and their uncertainties. *J. Geophys. Res.* 105, No. B12, 28,199–28,211.
- Paulson, A., Zhong, S., Wahr, J., 2005. Modelling post-glacial rebound with lateral viscosity variations. *Geophys. J. Int.* 163 (1), 357–371.
- Peltier, W.R., 1976. Glacial isostatic adjustment II. The inverse problem. *Geophys. J. Royal Astron. Soc.* 46, 669–706.
- Peltier, W.R., 1998. Postglacial variations in the level of the sea: implications for climate dynamics and solid-earth geophysics. *Rev. Geophys.* 36, 603–689.
- Peter, D., Tape, C., Boschi, L., Woodhouse, J.H., 2007. Surface wave tomography: global membrane waves and adjoint methods. *Geophys. J. Int.* 171 (3), 1098–1117.
- Poirier, J.P., 1985. *Transformation Plasticity, in Creep of Crystals*. Cambridge University Press, Cambridge, pp. 213–228.
- Reichenberg, I., 1973. *Evolutionsstrategie: Optimierung technischer Systeme nach Prinzipien der biologischen Evolution*. Fromann-Holzboog, Stuttgart-Bad Cannstatt.
- Resovsky, J.S., Ritzwoller, M.H., 1999. Regularization uncertainty in density models estimated from normal mode data. *Geophys. Res. Lett.* 26, 2319–2322.
- Resovsky, J.S., Trampert, J., 2003. Using probabilistic seismic tomography to test mantle velocity-density relationships. *Earth Planet. Sci. Lett.* 215, 121–134.
- Ricard, Y., Fleitout, L., Froidevaux, C., 1984. Geoid heights and lithospheric stresses for a dynamic earth. *Ann. Geophys.* 2, 267–286.
- Ricard, Y., Vigny, C., Froidevaux, C., 1989. Mantle heterogeneities, geoid, and plate motion: a Monte Carlo inversion. *J. Geophys. Res.* 94, 13, 739–13, 754.
- Ricard, Y., Wuming, B., 1991. Inferring the mantle viscosity and its three dimensional structure from geoid, topography and plate velocities. *Geophys. J. Int.* 105, 561–571.
- Richards, M.A., Hager, B.H., 1984. Geoid anomalies in a dynamic Earth. *J. Geophys. Res.* 89, 5987–6002.
- Richards, M.A., Hager, B.H., 1989. Effects of lateral viscosity variations on geoid anomalies and topography. *J. Geophys. Res.* 94, 10, 299–10, 313.
- Ritsema, J., van Heijst, H.J., Woodhouse, J.H., 1999. Complex shear wave velocity structure imaged beneath Africa and Iceland. *Science* 286, 1925–1928.
- Ritsema, J., van Heijst, H.J., Woodhouse, J.H., 2004. Global transition zone tomography. *J. Geophys. Res.* 109, Art. No. 02302.
- Romanowicz, B., 2001. Can we resolve 3D density heterogeneity in the lower mantle? *Geophys. Res. Lett.* 28, 1107–1110.
- Romanowicz, B., 2003. Global mantle tomography: progress status in the past 10 years. *Annu. Rev. Earth Planet. Sci.* 31, 303–31, 328 doi:10.1146/annurearth.31.091602.113555.
- Sammis, C.G., Dein, J.L., 1974. On the possibility of transformational superplasticity in the Earth's mantle. *J. Geophys. Res.* 79.
- Simmons, N.A., Forte, A.M., Grand, S.P., 2007. Thermochemical structure and dynamics of the African superplume. *Geophys. Res. Lett.* 34, L02301 doi:10.1029/2006GL028009.
- Smyth, J.R., 1987. Beta-Mg₂SiO₄: a potential host for water in the mantle. *Am. Miner.* 72, 1051–1055.
- Smyth, J.R., Jacobsen, S.D., 2006. Nominally anhydrous minerals and Earth's deep water cycle. In: van der Lee, S., Jacobsen, S.D. (Eds.), *Earth's Deep Water Cycle*, *Geophys. Monogr. Ser.*, vol. 168. Am. Geophys. Union, pp. 1–11.
- Spada, G., Sabadini, R., Yuen, D.A., 1991. Viscoelastic response of a hard transition zone: effects on post-glacial uplifts and rotational signatures. *Earth Planet. Sci. Lett.* 105, 453–462.
- Steinberger, B., O'Connell, R.J., 1997. Changes of the Earth's rotation axis owing to advection of mantle density heterogeneities. *Nature* 387, 169–173.
- Tapley, B., Ries, J., Bettadpur, S., Chambers, D., Cheng, M., Condi, F., Gunter, B., Kang, Z., Nagel, P., Pastor, R., Pekker, T., Poole, S., Wang, F., 2005. GGM02—an improved Earth gravity field model from GRACE. *J. Geodesy* doi:10.1007/s00190-005-0480-z.
- Tarantola, A., 1984. Inversion of seismic reflection data in the acoustic approximation. *Geophysics* 49, 1259–1266.
- Trampert, J., Deschamps, F., Resovsky, J., Yuen, D., 2004. Probabilistic tomography maps chemical heterogeneities throughout the lower mantle. *Science* 306, 853–856.

- Tromp, J., Tape, C., Liu, Q., 2005. Seismic tomography, adjoint methods, time reversal and banana-doughnut kernels. *Geophys. J. Int.* 160, 195–216.
- van der Hilst, R.D., Karason, H., 1999. Compositional heterogeneity in the bottom 1000 km of Earth's mantle: towards a hybrid convection model. *Science* 283, 1885–1888.
- van der Meijde, M., Marone, F., Giardini, D., van der Lee, S., 2003. Seismic evidence for water deep in Earth's upper mantle. *Science* 300, 1556–1558.
- Wessel, P., Smith, W.H.F., 1991. Free software helps map and display data. *Eos Trans., AGU* 725, 445–446.
- Wu, P., 1992. Deformation of an incompressible viscoelastic flat earth with power-law creep: a finite element approach. *Geophys. J. Int.* 108, 136–142.
- Zhang, S., Christensen, U.R., 1993. Some effects of lateral viscosity variations on geoid and surface velocities induced by density anomalies in the mantle. *Geophys. J. Int.* 114, 531–547.